Title

Bimorph deformable mirror: an appropriate wavefront corrector for retinal imaging?

Authors

Laut, Sophie
Jones, Steve
Park, Hyunkyu
et al.

Publication Date

2005-11-09

DOI

10.1117/12.630961

Peer reviewed

Bimorph deformable mirror: an appropriate wavefront corrector for retinal imaging?

Sophie Laut[*], Steve Jones[†], Hyunkyu Park[‡], David A. Horsley[‡], Scot Olivier[†], John S. Werner[*]

[*] University of California Davis, Department of Ophthalmology and Vision Science,
4860 Y Street, Sacramento, CA 95817
Phone (916)-734-6817, jswerner@ucdavis.edu, Phone (916)-734-5839, splaut@ucdavis.edu

[†] Lawrence Livermore National Laboratory, 7000 East Avenue, Livermore, CA 94550
Phone (925)-424-4777, stvnjns@llnl.gov , Phone (925)-423-6483, olivier1@llnl.gov

[‡] University of California Davis, Department of Mechanical and Aeronautical Engineering,
One Shields Avenue, Davis, CA 95616
Phone (530)-752-1778, dahorsley@ucdavis.edu

The purpose of this study was to evaluate the performance of a bimorph deformable mirror from AOptix, inserted into an adaptive optics system designed for *in-vivo* retinal imaging at high resolution. We wanted to determine its suitability as a wavefront corrector for vision science and ophthalmological instrumentation. We presented results obtained in a closed-loop system, and compared them with previous open-loop performance measurements. Our goal was to obtain precise wavefront reconstruction with rapid convergence of the control algorithm. The quality of the reconstruction was expressed in terms of root-mean-squared wavefront residual error (RMS), and number of frames required to perform compensation. Our instrument used a Hartmann-Shack sensor for the wavefront measurements. We also determined the precision and ability of the deformable mirror to compensate the most common types of aberrations present in the human eye (defocus, cylinder, astigmatism and coma), and the quality of its correction, in terms of maximum amplitude of the corrected wavefront. In addition to wavefront correction, we had also used the closed-loop system to generate an arbitrary aberration pattern by entering the desired Hartmann-Shack centroid locations as input to the AO controller. These centroid locations were computed in Matlab for a user-defined aberration pattern, allowing us to test the ability of the DM to generate and compensate for various aberrations. We conclude that this device, in combination with another DM based on Micro-Electro Mechanical Systems (MEMS) technology, may provide better compensation of the higher-order ocular wavefront aberrations of the human eye.

1. INTRODUCTION

High performance optical systems for retinal imaging have demonstrated improved lateral resolution by incorporating aberration correction with adaptive optics (AO). Ophthalmic instruments of the next decade are likely to include AO correction in combination with the architectures of classical retinal imaging systems, such as the fundus camera, scanning laser ophthalmoscope (SLO) or optical coherence tomography (OCT). A major impediment to achieving this goal in clinical instrumentation is the high cost and large size of conventional wavefront correctors.

The three key components of an AO system are the wavefront sensor, the wavefront corrector and the system controller. The Hartmann-Shack sensor (HS-WFS) is the wavefront sensor of choice in ophthalmic applications; however, special attention must be given to the choice of the parameters of the lenslet array which determines the ultimate capability of the AO system to detect a certain quantity of aberration.

Wavefront correctors for ophthalmic applications have included conventional deformable mirrors (DM) [1], liquid crystal spatial light modulators [2], micro-electro-mechanical systems (MEMS) [3], and

Smart Medical and Biomedical Sensor Technology III, edited by Brian M. Cullum, J. Chance Carter,
Proc. of SPIE Vol. 6007, 60070Q, (2005) · 0277-786X/05/$15 · doi: 10.1117/12.630961

Bimorph DMs [4]. The choice of wavefront corrector will have dramatic effects on the performance of the final correction, speed of the control loop, and convenience in the manipulation of the final instrument.

The purpose of this study is to characterize the performance of a Bimorph DM for wavefront compensation. We have previously characterized this device with "open-loop" control [5]; here, we describe its performance in "closed-loop" control mode. The latter reflects the intended application in AO imaging and also permits an analysis of controller optimization. To these ends, the paper first describes the "closed-loop" working optical set-up used for testing the mirror. Second, we validate our generator of synthetic wavefronts, and our wavefront reconstructor and analyzer. Third, we determine the range of amplitudes for each aberration type that our Hartmann-shack wavefront sensor is able to detect, and thereby outline the limitations of our system correction. Then, we show the performance of the wavefront corrector for aberrations included within these limits. This performance is described in terms of root-mean-square (RMS) residual wavefront error, peak-to-valley value (P-V), and time to achieve an acceptable compensation. From these studies, we outline and conclude on the limitation of our controller, based also on a "Least-Mean-Squares" method.

2. OPTICAL TESTBED AND CALIBRATION

2.1. Optical set-up

Figure 1 shows the components of the optical system used for the characterization of the bimorph deformable mirror. The DM is conjugated to the entrance pupil plane and the lenslet array. The entrance pupil of the system is imaged first onto the DM by a telescope composed of 2 lenses with 150 mm focal lengths; from the surface of the DM, the entrance of the system is re-imaged by a second telescope composed of 2 lenses with 200 mm focal lengths. Hence, the total transverse and longitudinal magnification ratios of the system are both equal to 1. Consequently, the wavefront detected by the wavefront sensor is identical to the one present in the entrance pupil of the system. The Hartmann-Shack wavefront sensor (HS-WFS) is a 10x10 lenslet array associated with a CCD camera (Dalsa CA-D4) positioned in the focal plane of the lenslets. The pitch of the array is 1 mm and the focal length of each lenslet is 55 mm. The camera acquires and refreshes the image of the wavefront at a rate of 16 frames/s. Because the camera frame-rate is slow in comparison to the maximum rate at which the DM control voltages may be updated, the camera frame-rate determines the maximum speed of the control loop. For simplicity, the time allotted for control computations is approximately equal to time required for the camera to acquire and transfer each image to the frame-grabber (PIXCI D PCI), such that the CCD camera is grabbing the next image as the calculations are done. For the purpose of this study, 16 frames/s is acceptable. However, it should be noted that in the case of aberration compensation of a real eye, the camera should refresh or at least be able to grab images at rates of ~ 25 frames/s [6].

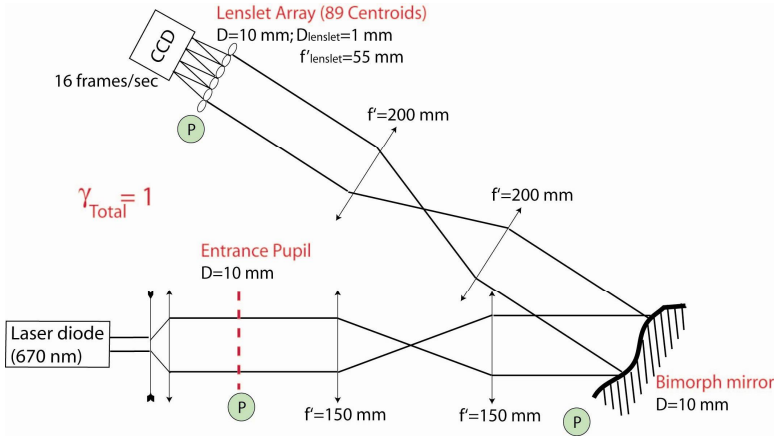

Figure 1 : ***Optical set-up of the AO system, illustrating the different Pupil planes.***

The bimorph DM studied in this paper is from AOptix, Inc. (cf. figure 2). This DM was originally manufactured for use in a laser telecommunication system, but has been reconfigured as a stand-alone unit for use in general AO applications. The DM is a 20 mm diameter disk composed of an electrostrictive ceramic, lead magnesium niobate (PMN), which is patterned with 35 actuator electrodes. Voltage applied to the actuator electrodes creates a local deformation of the DM surface. A 10-mm pupil defines the useful surface of the DM; the 19 actuators within the pupil are used to create surface curvature while the 16 outer actuators used to produce slope at the edge of the mirror. The 10-mm pupil makes this DM well-suited for vision science since it is slightly larger than the 7-mm entrance pupil of a dilated human eye. A limitation of bimorph DMs is that their stroke diminishes with increasing spatial frequency. We have previously demonstrated that this DM can produce ±3D of defocus; our goal here is to determine the ability of the device to correct for higher order aberrations.

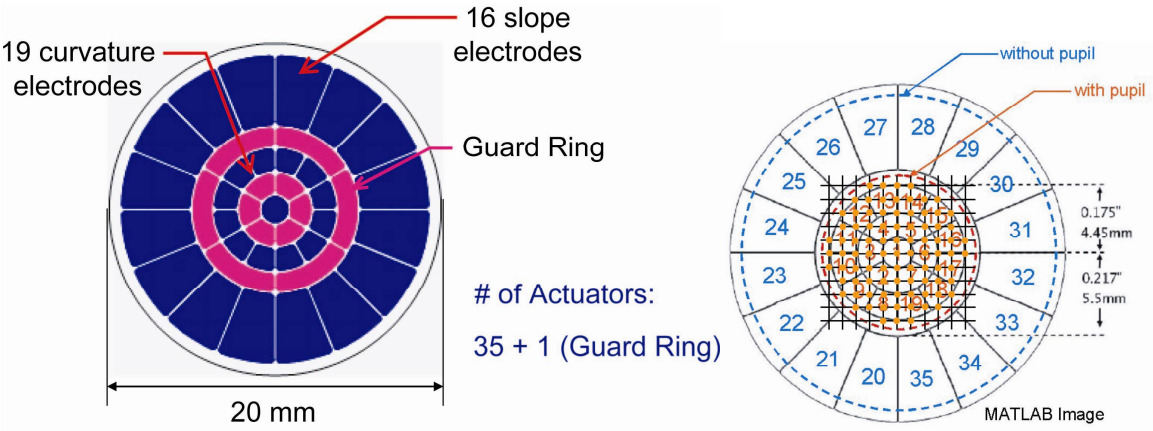

Figure 2 : ***a) Description of the different types of actuator composing the bimorph DM; b) Disposition of the lenslet array pupil plane versus the position of the actuators onto the bimorph DM.***

Figure 2 b) displays the distribution of the lenslet array vs. the position of the DM actuators. As we have already reported in a previous paper, an optimal number of 2 lenslets per actuator would assure good control of each actuator, eliminating the risk of the waffle modes which are undetectable by the wavefront sensor, and at the same time would reduce background noise, allowing correct detection of the centroid within each cell. In our case, the number of lenslets per actuator varies over the range of 1 to 5. The method used for detecting centroids within the acquired image consists to a simple center-of-mass process associated with a fixed threshold for elimination of the background noise. The determination of this threshold is the result of a preliminary calibration of the camera.

2.2. Calibration of the system: determination of the mirror "flat"

When all the actuators are set to a value of 0 V, the surface of the DM is not flat, but instead mostly parabolic (cf. figure 3). We estimate the corresponding wavefront amplitude to be 3.93 µm peak-to-valley, with an RMS of 1.29 µm composed mostly of defocus (Z4) and astigmatism (Z3). The peak-to-valley residual wavefront after Zernike fitting is around 1.75 µm, which means that after subtracting the defocus and astigmatism terms, the residual part of the wavefront is not representable by the first 20 Zernike modes and will contribute to the final wavefront error of the system. We verify this hypothesis in the next 2 paragraphs: hence the peak-to-valley of the residual wavefront error of the system, after Zernike fitting, is around 1.4 µm,

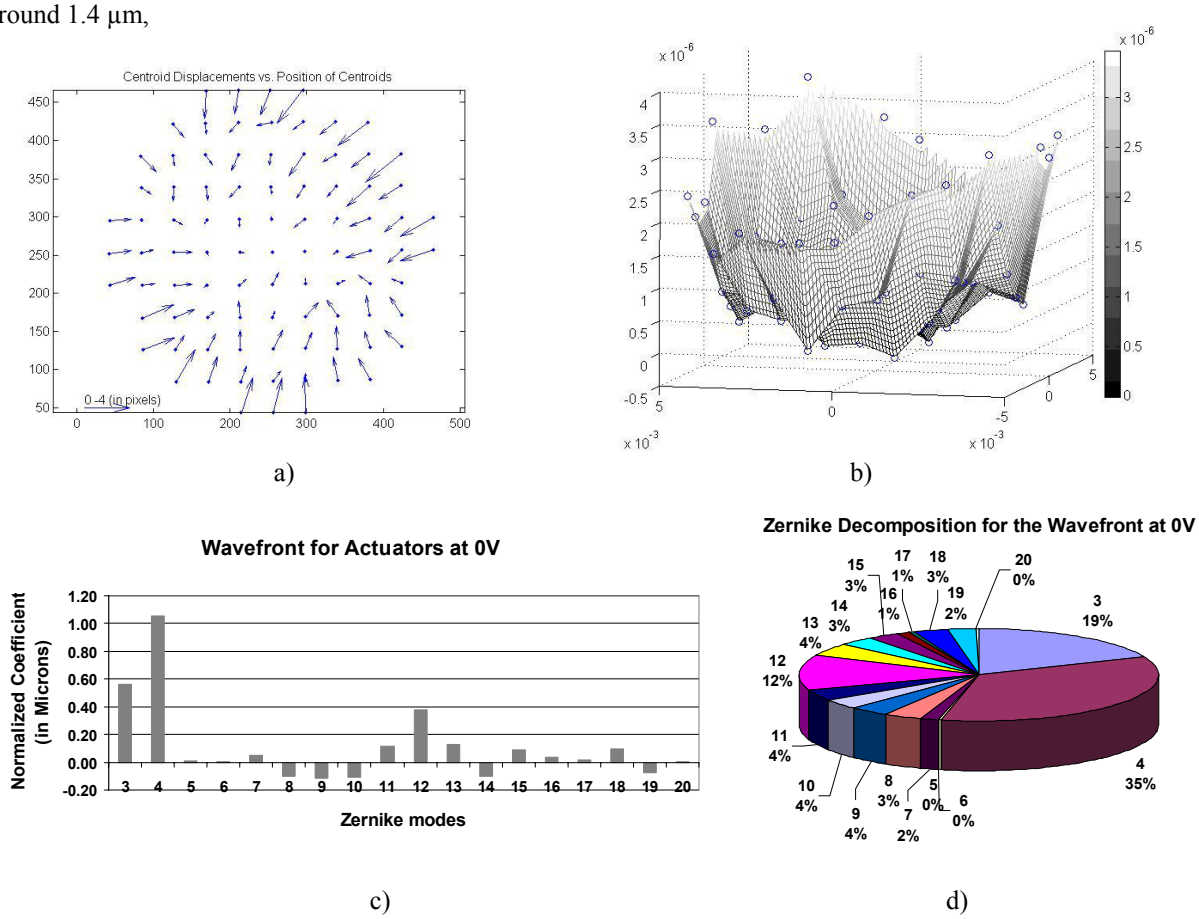

Figure 3 : ***a) Vectors slope of the wavefront when all actuators are at 0V; b) 3-D view of the corresponding reconstructed wavefront; c) and d) Decomposition of the wavefront with a 20 terms Zernike expansion.***

To compensate for positive as well as negative wavefronts, we used an iterative process to determine the set of voltages required to flatten the surface of the DM. The quality of the flatness of the wavefront achieved through this process determines the residual error of the system and the quality of our ultimate aberration compensation. As a first step, we recorded a reference wavefront measurement with the DM replaced by a precision flat mirror; we judged that a λ/10 flat mirror was sufficient, as we made flatness measurements using a 2-faced λ/10 parallel plate. Then, with the DM in the system, we began to iteratively flatten the mirror. In each iteration, we recorded a system matrix of influence functions, consisting of successive wavefront measurements by the HS-WFS when each actuator is successively pushed and pulled

to a certain value while the other actuators are held at a constant voltage of 0 V. Next, the control loop was closed, driving the RMS wavefront error close to zero and forcing the DM to a flatter surface. The process was then repeated, recording a new system matrix before closing the control loop again. With each iteration, the DM surface more closely approaches the ideal flat surface. After a few loops, the "flat" is judged acceptable, and the system is ready to compensate for any exterior aberrated wavefront.

The residual error of the system is finally described in figure 4. The RMS value is equal to 0.27 µm (~0.4λ) with a Peak-to-Valley equal to 1.4 µm. The residual wavefront is mostly composed of aberrations higher than Zernike mode 9. This result is not surprising: the bimorph DM is expected to perform best when correcting low-order aberrations such as astigmatism, defocus, and coma. The higher-order modes appear obviously less well corrected, the worst cases being Zernike modes 15 and 19.

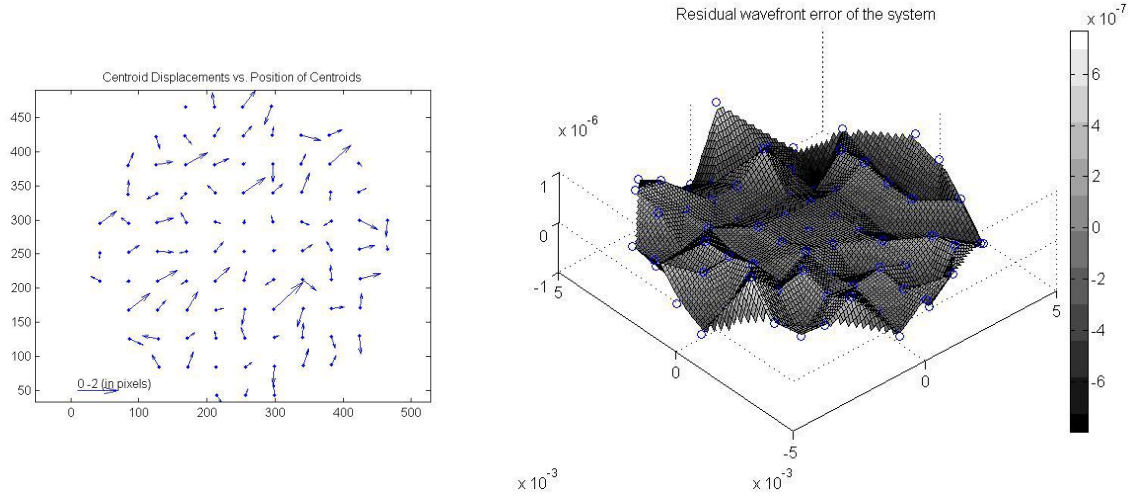

a) b)

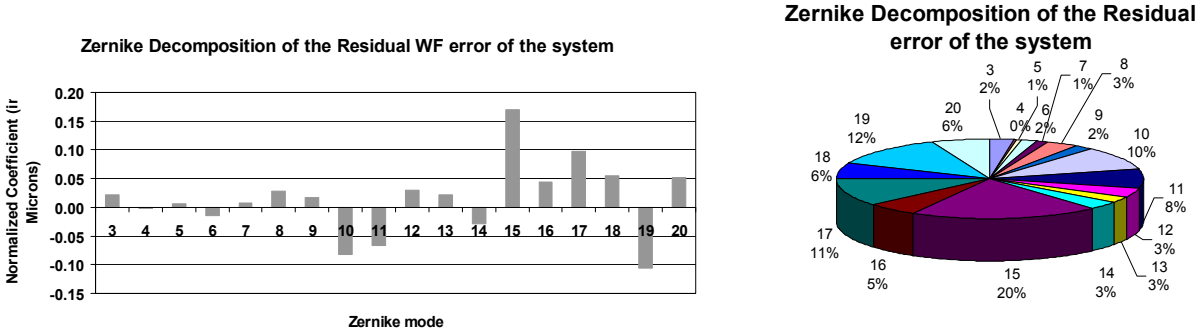

c) d)

Figure 4 : ***a) Vectors slope of the residual wavefront error of the system after correction; b) 3-D view of the corresponding reconstructed wavefront; c) and d) Decomposition of the wavefront with a 20 term Zernike expansion.***

3. VALIDATION OF THE WAVEFRONT GENERATOR, WAVEFRONT RECONSTRUCTOR AND WAVEFRONT ANALYZER

We used two methods to test the ability of our system to correct for various wavefront aberrations. First, we physically introduced spherical and cylindrical trial lenses in the entrance pupil of our system to demonstrate the correction of low-order aberrations. Second, since it is difficult to physically introduce precisely-defined higher-order aberrations, we utilized a computational method to generate synthetic wavefronts. In this section, we check the precision of our methods for the generation of synthetic wavefronts. We show the precision of our wavefront reconstruction from the measurements of the centroid displacements. We will check also the results of our analysis for the reconstructed wavefronts by a Zernike decomposition fitting. For these purposes, we use the measurements recorded from the wavefront sensor for a set of sphere and cylinder trial lenses, placed into the entrance pupil plane of the system.

3.1. Wavefront generator and reconstructor

To be able to measure the quality of compensation of the DM for Zernike modes higher than mode 5 (astigmatism), we first developed a computational model which predicts the locations of the centroids on the HS-WFS as the result of an aberration described by a particular Zernike coefficient value. The resulting centroid locations (in pixels) corresponding to the desired Zernike mode are input to the AO system controller as a residual wavefront error. When the AO loop is closed, the controller attempts to drive the *measured* centroid locations to the *desired* centroid locations, forcing the DM to achieve the conjugate phase profile for the input aberration.

To validate our wavefront generator, we produced synthetic defocus wavefronts corresponding to the same focal lengths as the experimentally-measured spherical trial lenses. We then compared the computed wavefront error resulting from each synthetic wavefront with the measured error resulting from the corresponding trial lens. The experimental data is measured in terms of HS-WFS centroid displacements (in pixels), which corresponds to the local slope of the wavefront. Thus, the measured centroid variance is linearly proportional to the RMS wavefront error, but the scale-factor relating these two parameters is different for each Zernike mode. Figure 5 shows a plot of the measured and synthetic centroid variance for the various trial lenses versus their RMS wavefront error. We note that there is close correspondence between the synthetic and measured aberrations.

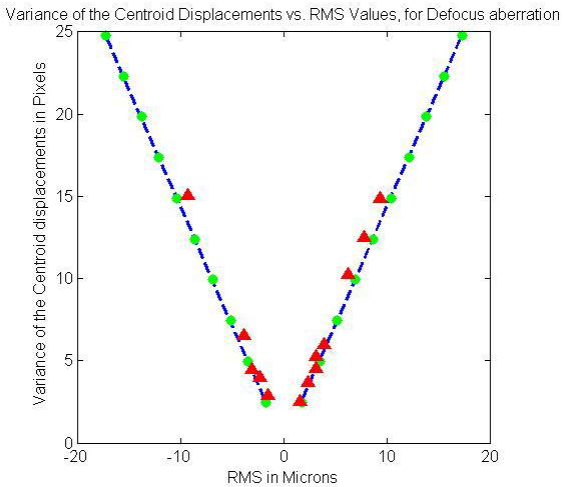

Figure 5 : ***Comparison of the variance of the centroid displacements versus the RMS values for experimentally-measured Spherical Trial lenses (triangles) and synthetic wavefronts (dots).***

3.2. Wavefront reconstructor and analyzer

Tables 1 and 2 show calculated and experimentally measured values for the Zernike coefficients, RMS wavefront error, and peak-to-valley wavefront error for both the spherical and cylindrical trial lenses. Calculated values are based on the focal length of each lens. The experimental data was preprocessed using the following procedures. First, in the case of large amplitude aberrations, we observed that the large wavefront slope causes a certain number of centroids to move outside the cells defined on the HS-WFS, resulting in missing centroid data. Thanks to the use of an extrapolation algorithm, we first re-estimated these corresponding displacements (cf. figure 6). In a second step, we correct for any translational misalignment of the wavefront relative to the center of the wavefront sensor pupil plane by removing any x and y axis offset value present in the entire set of centroid displacements. In a last step, we remove any tilt present in the reconstructed wavefront; this tilt is mainly due to misalignments introduced into the system after calibration once we switch from the flat mirror to the DM. The processed wavefront is then fit with a 5^{th}-order polynomial and re-expressed in Zernike terms. As we can see in Table 1, the results measured for the set of positive and negative spherical trial lenses are close to the expected values. Table 1 also shows the residual wavefront error after fitting the measured wavefront with a 5^{th}-order Zernike expansion. This residual error is approximately the same as the value obtained during system calibration using the flat mirror. The same approach was also used for the estimation of the cylinder values from the centroid displacements file (cf. table 2 and figure 7). Because cylinder is a combination of astigmatism and defocus (Zernike modes 3, 4 and 5), we have included calculated and measured values for these three Zernike coefficients.

Value of the Trial lens (D)	Expected nonNormalized Coef. (Microns)	Expected RMS (Microns)	Expected Peak-to-Valley (Microns)	Estimated Value (D)	Measured nonNormalized Coef. (Microns)	Measured RMS (Microns)	Measured Peak-to-Valley (Microns)	Residual WF Peak-to-Valley (Microns)	Missing centroids
-1.50	-5.41	-9.38	-18.75	**-1.49**	-5.35	9.31	20.56	1.66	12
-1.00	-3.61	-6.25	-12.50	**-1.02**	-3.67	6.36	14.45	1.09	0
-0.62	-2.24	-3.88	-7.75	**-0.65**	-2.35	4.09	9.02	1.27	0
-0.37	-1.34	-2.31	-4.63	**-0.40**	-1.42	2.51	5.63	1.10	0
-0.25	-0.90	-1.56	-3.13	**-0.28**	-1.02	1.78	3.99	0.95	0
0.25	0.90	1.56	3.13	**0.25**	0.87	1.55	3.64	0.95	8
0.37	1.34	2.31	4.63	**0.37**	1.30	2.29	5.37	1.23	10
0.50	1.80	3.13	6.25	**0.46**	1.64	2.86	6.40	2.22	9
0.62	2.24	3.88	7.75	**0.59**	2.11	3.66	8.22	1.31	0
1.00	3.61	6.25	12.50	**1.01**	3.63	6.31	13.52	1.16	1
1.25	4.51	7.81	15.63	**1.23**	4.41	7.66	17.54	1.83	2
1.50	5.41	9.38	18.75	**1.46**	5.27	9.14	21.62	2.01	14

Table 1 : ***Comparison of the expected optical powers, non normalized Zernike coefficients, RMS and peak-to-valley values in the case of a set of sphere trial lenses, with the estimated ones after measurements of the centroid displacements by the Hartman-Shack wavefront sensor.***

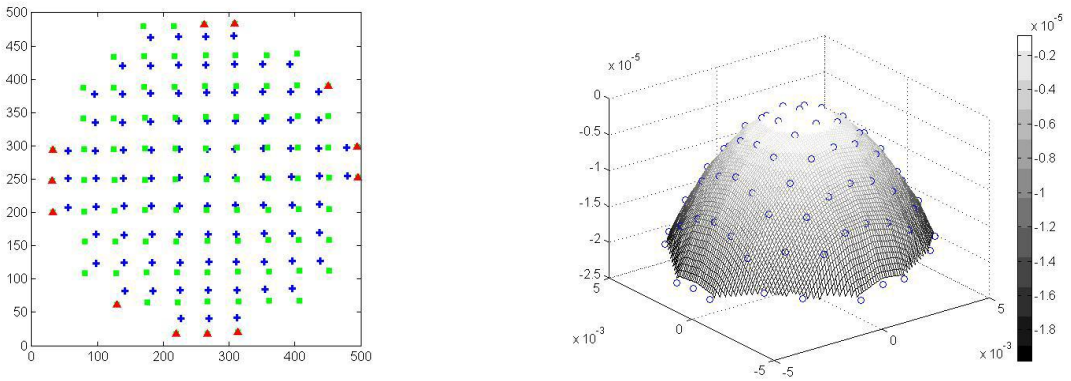

a) b)

Figure 6 : ***a) Example of centroid displacements in the Hartman-Shack pupil plane, in the case of a spherical trial lens. The crosses correspond to the reference positions of the centroids, the squares are the new positions describing point per point the Defocus aberration. The triangles are the extrapolated values in the case of missing centroids or incoherent measured centroid displacements; b) 3-D view of the corresponding wavefront reconstruction.***

Value of the Trial lens (D)	Measured nonNormalized Coef. a3 (Microns)	Measured nonNormalized Coef. a4 (Microns)	Measured nonNormalized Coef. a5 (Microns)	Angle of the Axis (Degrees)	Estimated Value for Defocus (D)	Estimated Value for Cylinder (D)	Missing centroids
-1.50	-0.40	-3.08	-3.78	**3.02**	**-2.20**	**-1.92**	9
-1.25	-1.50	-2.48	-2.89	**13.72**	**-1.77**	**-1.65**	1
-1.00	-0.90	-2.03	-2.45	**10.09**	**-1.45**	**-1.32**	0
-0.75	-0.82	-1.39	-1.78	**12.37**	**-0.99**	**-0.99**	0
0.25	-0.12	0.68	0.59	**-5.75**	**0.49**	**0.30**	0
0.50	0.83	0.94	0.95	**20.57**	**0.67**	**0.64**	0
1.00	0.82	1.69	1.45	**14.74**	**1.21**	**0.84**	0
1.25	3.43	2.45	-0.52	**49.30**	**1.75**	**1.75**	0
1.50	2.78	2.50	2.85	**22.14**	**1.79**	**2.01**	0
1.75	2.38	2.31	3.35	**17.70**	**1.65**	**2.08**	14

Table 2 : ***Comparison of the expected optical power, in the case of a set of cylinder trial lenses, with the estimated ones after measurements of the centroid displacements by the Hartman-Shack sensor.***

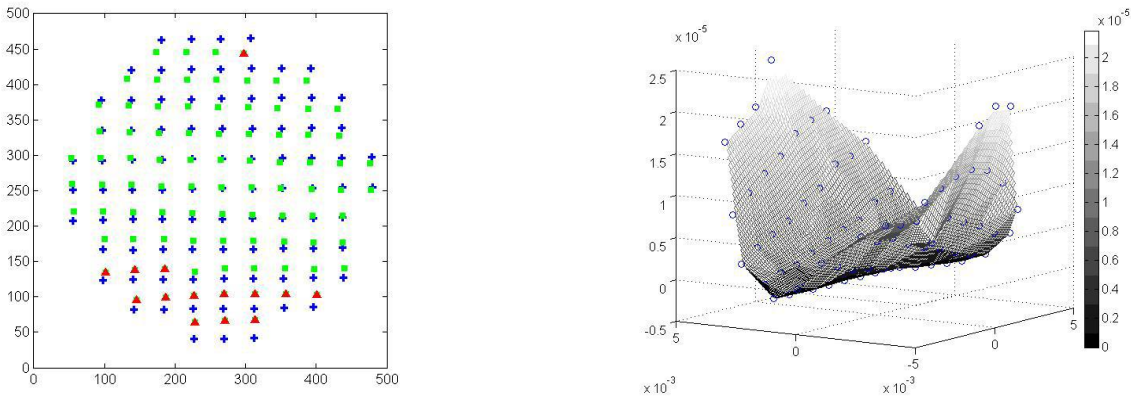

Figure 7 : ***a) Example of centroid displacements in the Hartman-Shack pupil plane, in the case of a cylinder trial lens. The crosses correspond to the reference positions of the centroids, the squares are the new positions describing the aberration. The triangles are the extrapolated values in case of missing***

centroids or incoherent measured centroid displacements; b) 3-D view of the corresponding wavefront reconstruction.

4. HARTMANN-SHACK WAVEFRONT SENSOR LIMITATIONS

Due to the finite size of the lenslet cells, each Zernike aberration may be detected over a limited range of amplitudes. Centroids that move outside the lenslet cell are missing from the centroid location data, affecting ability of the sensor to detect the aberration, and the ability of the AO controller to compensate for it. It appears important to determine the domain of validity of our sensor for each Zernike mode.
In the case of Defocus aberrations it is relatively easy to calculate this limit; the value depends on the lenslet characteristics in terms of focal length and pitch. We estimated that our system had a maximum observable defocus value of 1.82D and we experimentally confirmed this value by introducing successively a 1.75D and a 2D Trial lens into the system: the system managed to correct for the 1.75D defocus value but could not correct for the 2D value.

A possibility exists to partially overcome the limitation imposed by our wavefront sensor for detecting large amplitude defocus. The solution is to first introduce into the system a correctable value of defocus, holding the DM shape after AO compensation, then add a larger value of defocus and then re-close the AO loop. Thanks to this iterative technique, we managed to correct 2.25D by successively introducing trial lenses with 1D sphere power (variance of the centroid displacements equal to 10.51 pixels before correction and 0.58 pixels after correction), and then 2.25D (variance of the centroid displacements equal to 11.97 pixels before correction and 4.31 pixels after correction). If the 2.25D trial lens had been directly added into the system, the controller would not have been able to correct for it.

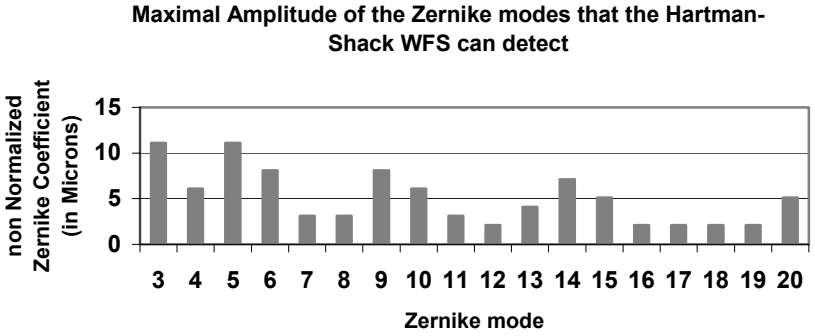

Figure 8 : ***Estimation of the maximal detectable amplitude of the wavefront by the Hartman-Shack wavefront sensor.***

By progressively increasing the Zernike coefficient values, generating the corresponding synthetic wavefront and controlling the quantity of displacement for each centroid, we can then get a rough approximation of the maximal amplitude detectable for each aberration by the HS-WFS. Figure 8 shows the results of our simulations: we observed that the sensitivity of our sensor progressively decreases with the increasing of the Zernike order. Hence, astigmatism appears to be observable on a larger range of values than defocus, the same for trefoil and coma. Spherical aberrations seem to be one of the least detectable modes, together with majority of the 5^{th} order Zernike modes.

5. COMPENSATION QUALITY OF THE BIMORPH DM

Using the information previously presented, we checked quantitatively the quality of compensation of the bimorph deformable mirror, in the case of aberrations expressed by a single Zernike mode. This quality is described in terms of variance of the centroid displacements (in pixels), RMS, and time required by the AO controller to compensate for the aberration (in number of HS-WFS frames).

5.1. Maximal wavefront amplitude value versus Zernike mode

The measurement principle we employed was to generate synthetic wavefronts corresponding to each Zernike coefficient with successively increasing amplitude. The synthetic wavefronts were then entered into the system as residual wavefront errors, the AO control loop was closed, and wavefront compensation was performed. Following convergence of the AO loop, we measured the residual wavefront error. We obtained charts similar to the ones displayed in figure 9 and figure 10, in the case of a Zernike mode 5 (astigmatism).

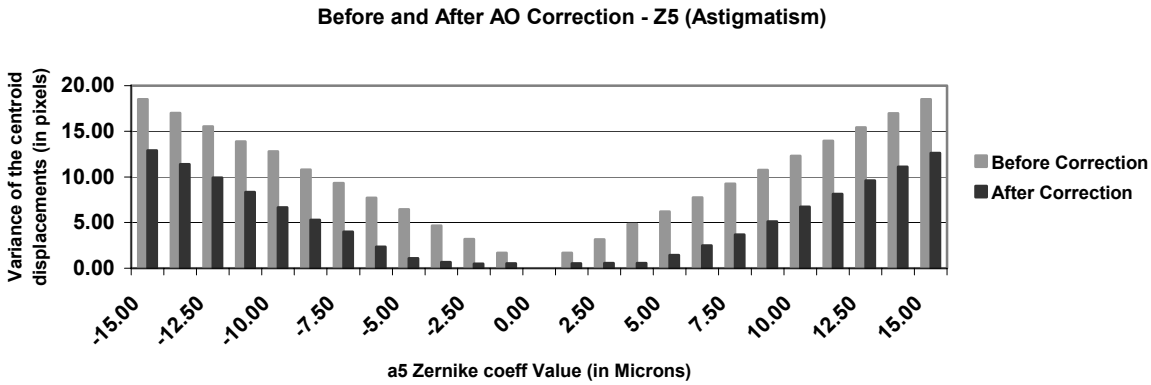

Figure 9 : ***Comparison of the centroid displacements variances, measured at the Hartman-Shack pupil plane, before and after AO compensation, in the case of a increasing amplitude of the non normalized Zernike coefficient values a5 for Astigmatism.***

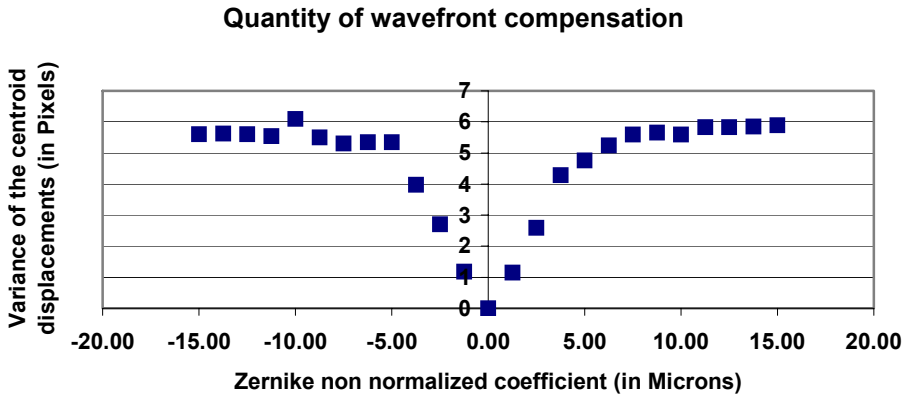

Figure 10 : ***AO system wavefront compensation performances in the case of Astigmatism aberrations; expressed in terms of variance values of the centroid displacements.***

From the figure 9 and figure 10, we can categorize the behavior of our system into 2 different operating regimes. In the first regime, corresponding to relatively small amplitude aberrations and Zernike coefficient values, the residual RMS error remaining after convergence of the AO loop is approximately constant. If we continue to increase the aberrations, we progressively exceed the correction capability of the system, and one-by-one the DM actuators become saturated, at which point we reach the maximal quantity of correction available for this Zernike mode. In the case of Zernike mode 3, this phenomenon occurs for a value of the non normalized Zernike coefficient equal to approximately 6.25 Microns. The quantity of the wavefront compensation, hence of centroid displacements, performed at this point corresponds roughly to 6 pixels for a signed aberration (7.2 Microns in RMS values for the 3rd Zernike mode).

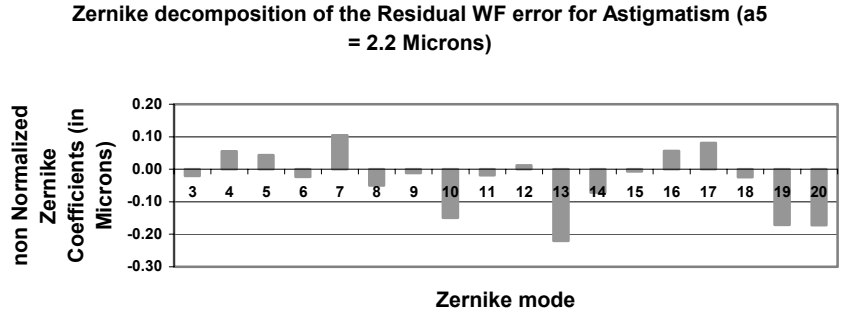

a)

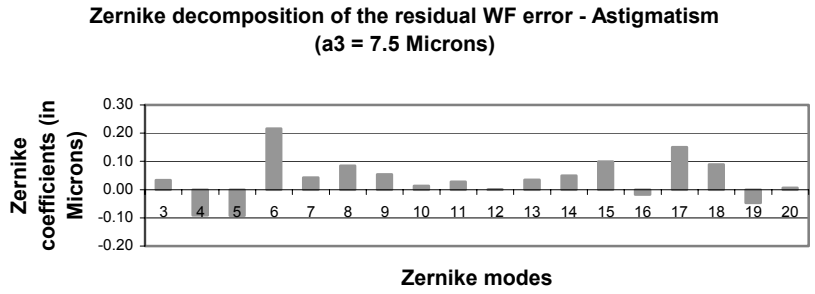

b)

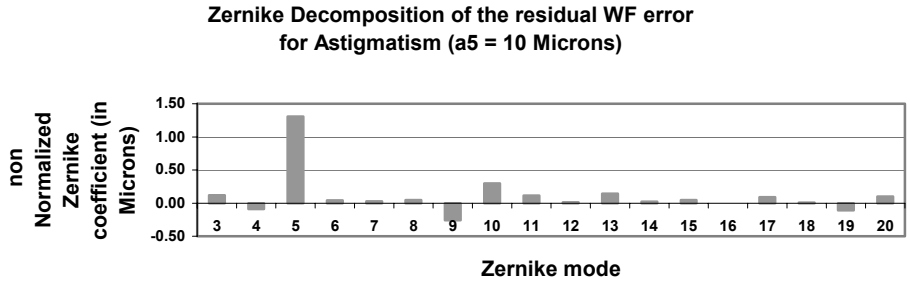

c)

Figure 11 : ***Zernike decomposition of the residual wavefront error in the case of the Astigmatism aberration compensation, with a non normalized coefficient value equals respectively to : a) 2.2 Microns (RMS = 0.41 µm; P-V = 1.31 µm; P-V Residual = 1.05 µm); b) -7.5 Microns (RMS = 0.35 µm; P-V = 1.68 µm; P-V Residual = 1.36 µm); c) 10 Microns (RMS = 1.4 µm; P-V = 4.03 µm; P-V Residual = 1.66 µm).***

Figure 11 shows the composition of the residual wavefront error when compensating for Astigmatism (Z5), in both the linear working mode of the system and when the system is saturated. Figure 12 summarizes the maximum compensation capability of the system for each Zernike mode. The results look very similar to the ones obtained by E. Dalimier and C. Dainty, published in their recent paper [7]. As expected, we note that the low order aberrations are compensated the best, with the maximal compensation amplitude diminishing progressively with increasing aberration order. The general shape of the graphic results look similar; however, our estimated values for Defocus and Astigmatism appear smaller than the ones obtained by E. Dalimier and C. Dainty.

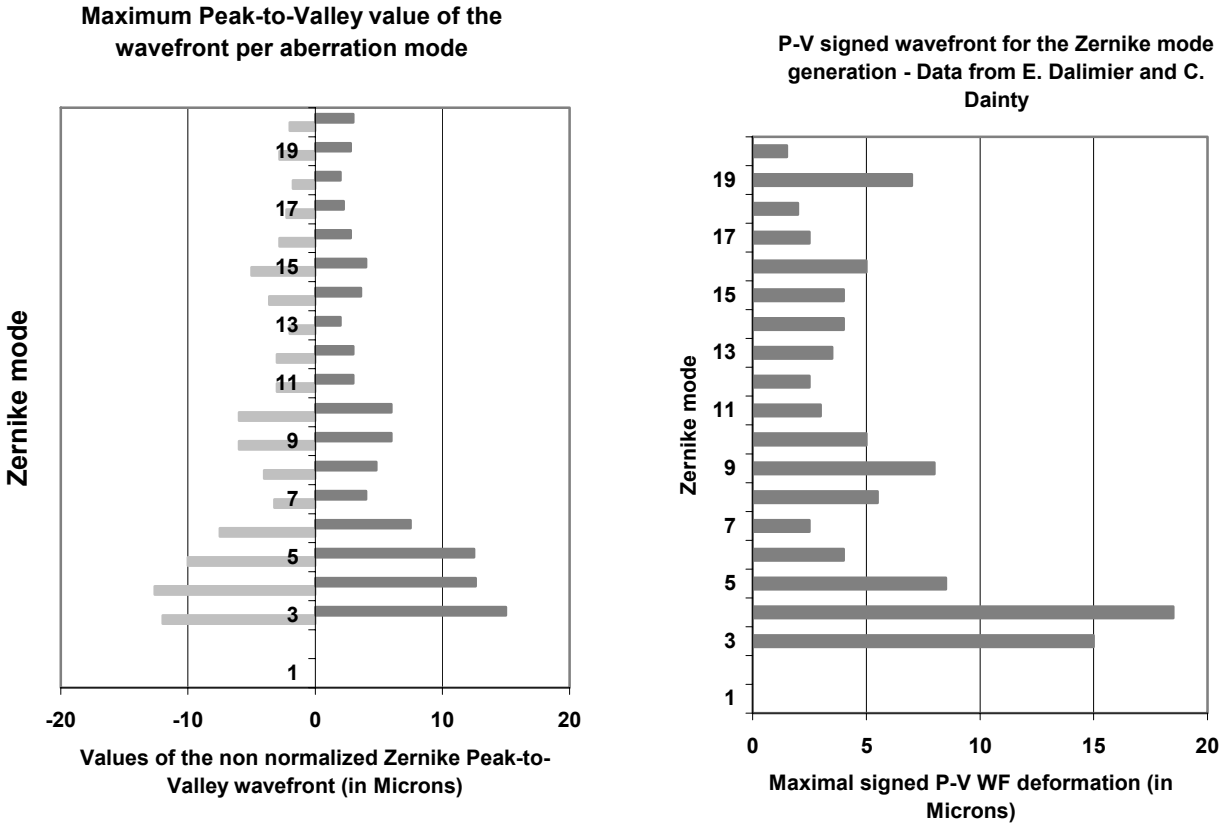

a) b)

Figure 12 : ***Comparison of our measured data (a), with data from E. Dalimier and C. Dainty (b), in terms of Peak-to-Valley values of the maximal wavefront generable by the bimorph DM.***

It is also interesting to compare our data with the ones obtained by our earlier open-loop characterization method (cf. Figure 13) [5]. Although we find general agreement between the open-loop data and the results produced by our closed-loop system, there is some difference between the amplitudes achieved for individual Zernike modes. This difference may be partly due to manufacturing variations between the two different DM units used for these measurements. More importantly, the open-loop measurements are limited by actuator saturation and are therefore expected to underestimate the maximum achievable correction. This effect is particularly apparent in the case of defocus, where the maximum correction amplitude is much smaller than expected.

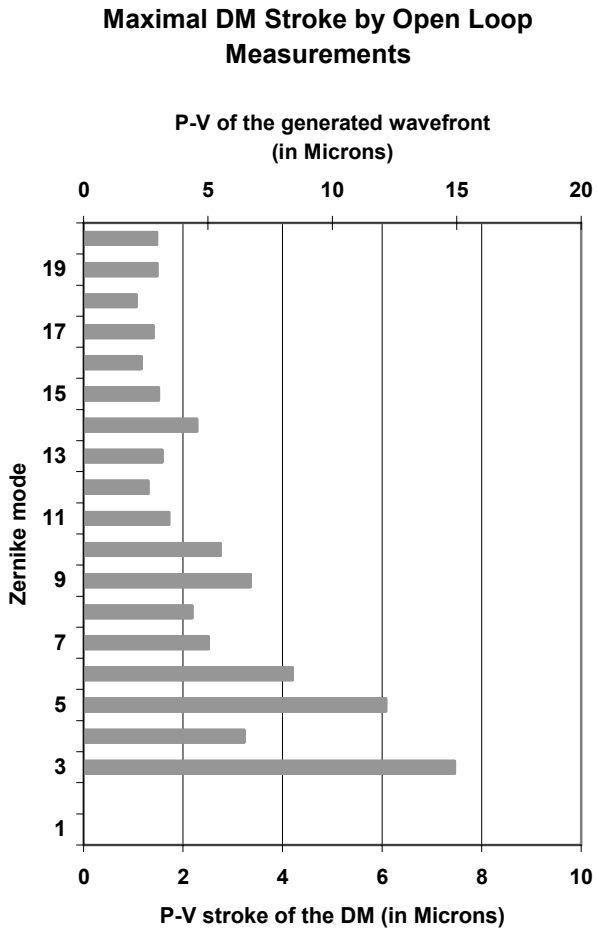

Figure 13 : ***Data from [5] describing the maximal Peak-to-Valley stroke of the bimorph DM for each Zernike mode. The data are also translated into the corresponding maximal Peak-to-Valley of the generable wavefront by the DM.***

5.2. Average estimated time for the wavefront compensation of each Zernike mode

We determined the convergence time required for the AO loop to compensate for a specific wavefront as a function of its amplitude, in the special case of an Astigmatism aberration Z5. We obtained the graph displayed in figure 14. In this chart and in figure 15, it is apparent that there is a difference in the system behavior for small aberration amplitudes versus for large aberration amplitudes. In the case of small aberrations, we observe a small amount of oscillations in the RMS error before convergence; these oscillations are absent in the case of larger aberrations. We attribute this difference to the fact that, for large aberrations, the DM is saturated before the optimal correction can be achieved. As a result, the error signal which drives the control loop does not change signs and no oscillations are observed. We note that the oscillatory behavior suggests that the coefficients of our PI controller may not be optimal for the present sampling rate and further study will be devoted to this issue.

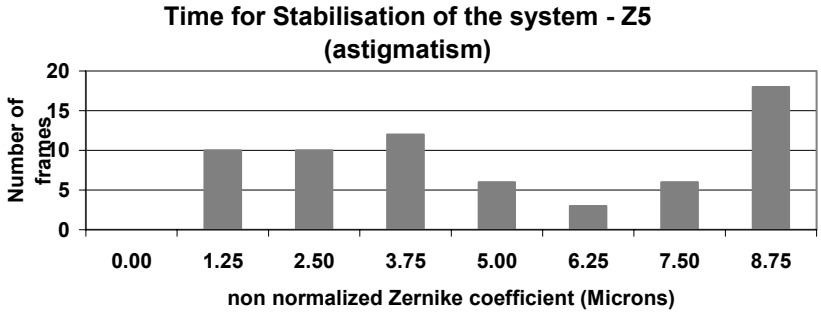

Figure 14 : ***Average number of frames before completing the compensation of a Astigmatism aberration Z5, for different Zernike coefficient values.***

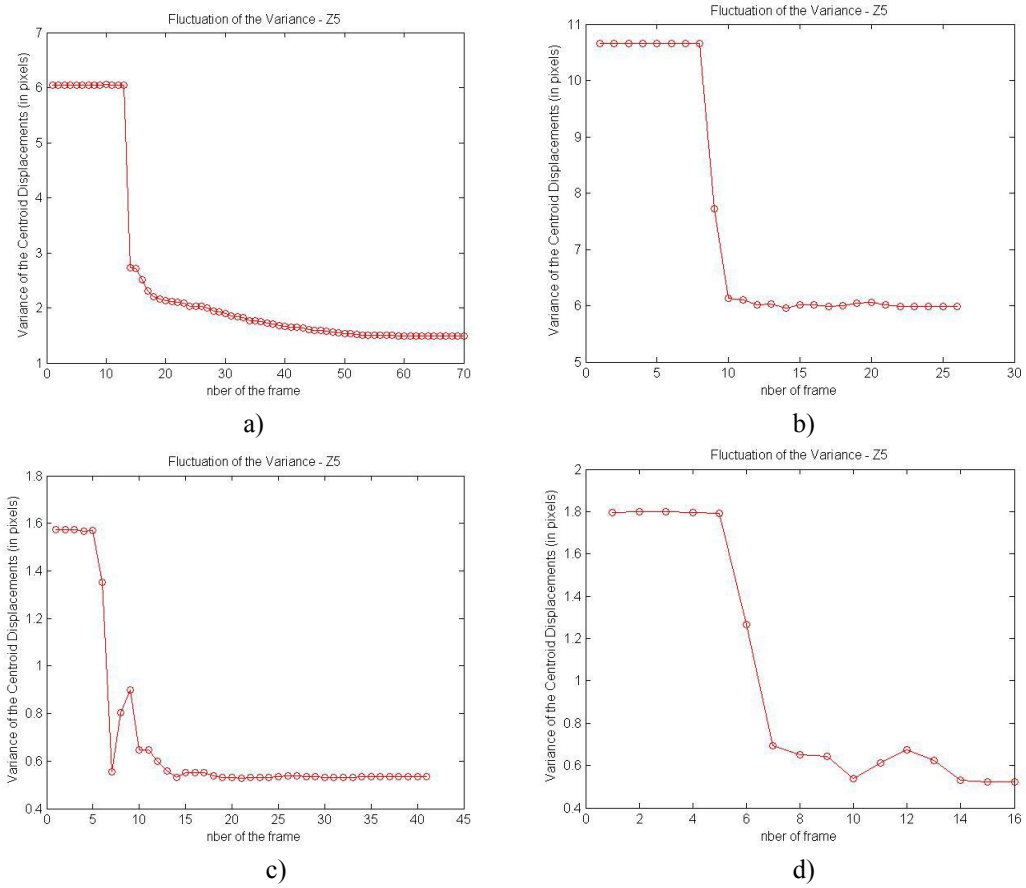

Figure 15 : ***Step responses of the system in the case of an increasing value of the a5 (Astigmatism) non normalized Zernike coefficient. a) a5 =5 µm; b) a5 =12.5 µm; c) a5 =1.25 µm; d) a5 = 3.75 µm.***

6. CONCLUSION

We studied the closed-loop response of an AOptix bimorph deformable mirror, and estimated its linear operating range in terms of variance of centroid displacements and hence RMS values, for each Zernike mode. The results obtained are consistent with the results previously presented in our earlier paper as well as the more recent paper from E. Dalimier and C. Dainty. As expected, we conclude that this kind of deformable mirror has a large amplitude response for low order aberrations but that its compensation

quality rapidly decreases with increasing Zernike coefficient values: the maximal correction obtained for a 2nd order Zernike mode, such as Defocus or Astigmatism, is roughly twice the correction which can be obtained for a 3rd order mode, such as Coma. The value diminishes by an additional factor of 2 in the case of a 4th order aberration, such as Spherical aberration, and by another factor 2 for a 5th order aberration. This mirror appears to be ideal for correcting the prescription of patients, but may rapidly become insufficient for compensating higher Zernike order aberrations. We may therefore consider cascading a second DM, such as a MEMS DM, which is more suited for the correction of higher order aberrations We also showed that the Hartman-shack wavefront sensor has its own limitation in terms of the range of detectable aberrations. We finally showed the convergence behavior of our PI-type AO controller. Further optimization of the controller, through a root-locus analysis, should lead to improved settling behavior. It would also be beneficial to make a deeper study of the DM compensation response for a combination of different Zernike modes, as in the case of a cylinder aberration.

ACKNOWLEDGEMENTS

Work supported by National Eye Institute grant (EY014743).

7. REFERENCES

[1] J. Z. Liang, D. R. Williams, and D. T. Miller, "Supernormal vision and high-resolution retinal imaging through adaptive optics," *Journal of the Optical Society of America a-Optics Image Science and Vision*, vol. 14, pp. 2884-2892, 1997.

[2] A. Awwal, B. Bauman, D. Gavel, S. Olivier, S. Jones, D. Silva, J. Hardy, T. Barnes, and J. Werner, "Characterization and Operation of a Liquid Crystal Adaptive Optics Phoropter," presented at Astronomical Adaptive Optics Systems and Applications, 2003.

[3] N. Doble and D. Williams, "The Application of MEMS Technology for Adaptive Optics in Vision Science," in *IEEE Journal of Selected Topics in Quantum Electronics*, vol. 10, 2004, pp. 629-635.

[4] H. Hofer, L. Chen, G.-Y. Yoon, B. Singer, Y. Yamauchi, and D. Williams, "Improvement in retinal image quality with dynamic correction of the eye's aberrations," *Optics Express*, vol. 8, pp. 631-643, 2001.

[5] D. A. Horsley, H. K. Park, S. P. Laut, and J. S. Werner, "Characterization for vision science applications of a bimorph deformable mirror using phase-shifting interferometry," *Proceedings of the SPIE*, vol. 5688, pp. 133-144, 2005.

[6] E. Fernandez and P. Artal, "Membrane deformable mirror for adaptive optics: performance limits in visual optics," *Optics Express*, vol. 11, pp. 1056-1069, 2003.

[7] E. Dalimier and C. Dainty, "Comparative analysis of deformable mirrors for ocular adaptive optics," *Optics Express*, vol. 13, pp. 4275-4285, 2005.